

LETTER TO THE EDITOR

A nanotherapeutic strategy to target drug-tolerant cells and overcome EGFR tyrosine kinase inhibitor resistance in lung cancer

Dear Editor,

For patients with epidermal growth factor receptor (*EGFR*) mutant non-small cell lung cancer (NSCLC), *EGFR* tyrosine kinase inhibitors (TKIs) are used as the first-line treatment [1, 2]. Despite initial therapeutic responses, patients invariably experience disease progression due to acquired drug resistance [3]. Resistance arises, in part, because a subset of cancer cells undergoes epithelial-mesenchymal transition (EMT) and remains viable despite exposure to *EGFR* TKI concentrations that eliminate the bulk population [4]. The surviving cells can be re-sensitized to treatment by prolonged culture in the absence of *EGFR* TKIs, indicating a transient, potentially reversible, tolerance to these drugs [4]. However, these drug-tolerant cells (DTCs) may regain proliferative potential, evolve, and give rise to diverse stable mechanisms of resistance in patients [5, 6]. To address this clinical challenge, we developed a novel liposomal nanodrug, Axl-LP-VD-CTA091, to inhibit DTCs, thus targeting the origin of diverse resistance mechanisms (Figure 1A). In this formulation, the pro-differentiation agents 1,25-dihydroxyvitamin D3 (VD) and CTA091 were co-encapsulated in liposomes (LP) (Figure 1B). VD was used to suppress EMT [7] that underlies drug tolerance. CTA091 prevented catabolic inactivation of VD by 24-hydroxylase [8]. Axl aptamers [9] enabled preferential targeting of nanodrug to DTCs, which are known to

have increased Axl expression [10] (see Supplementary Materials for experimental details).

We prepared Axl-LP-VD-CTA091 by encapsulating VD and CTA091 in LP and then conjugated Axl aptamers on the LP surface (Supplementary Figure S1A). The size and zeta potential of Axl-LP-VD-CTA091 were 106 ± 3 nm and $+30.9 \pm 3.8$ mV, respectively (morphology and size distribution in Supplementary Figure S1B). The encapsulation efficiency of VD and CTA091 was 75%. Axl-LP-VD-CTA091 were stable for 24 h \pm serum (Supplementary Figure S1C).

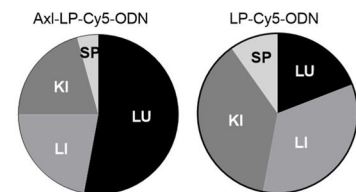
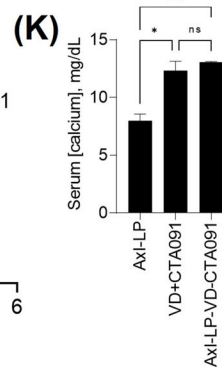
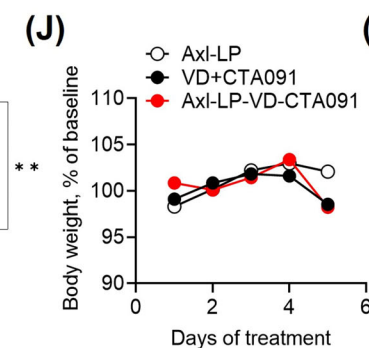
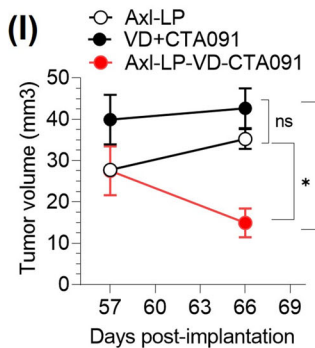
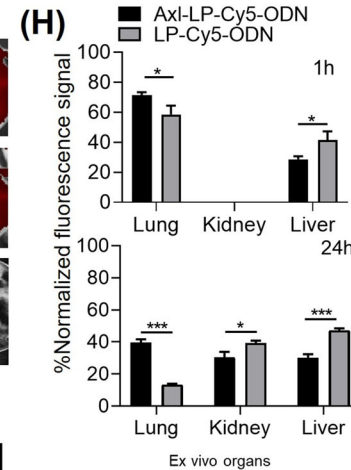
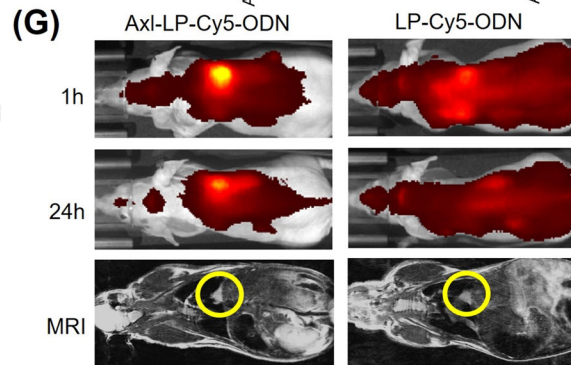
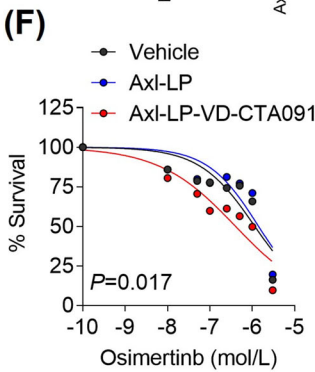
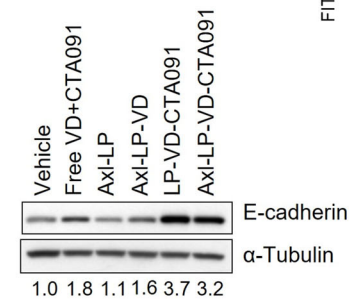
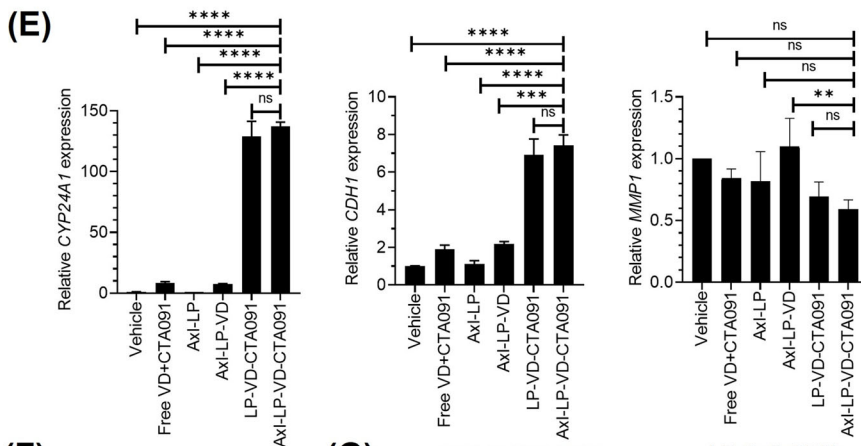
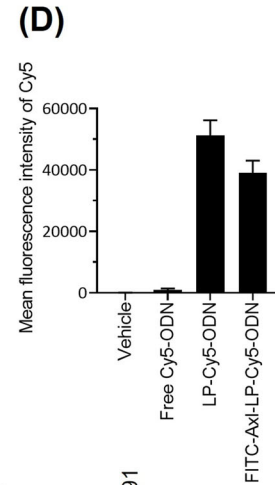
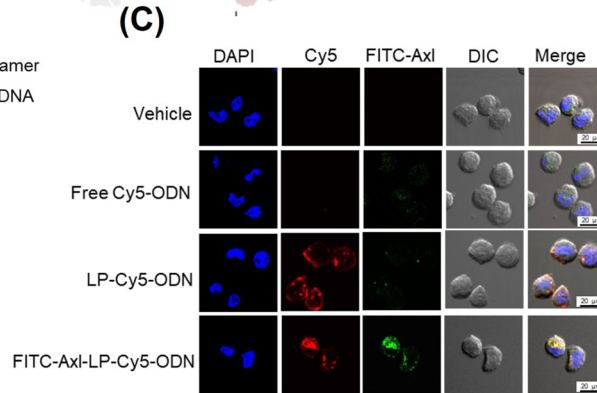
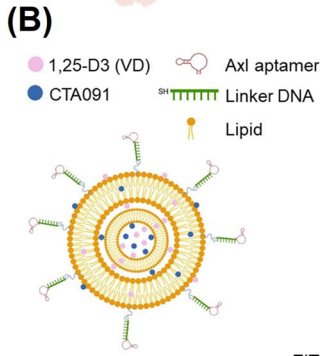
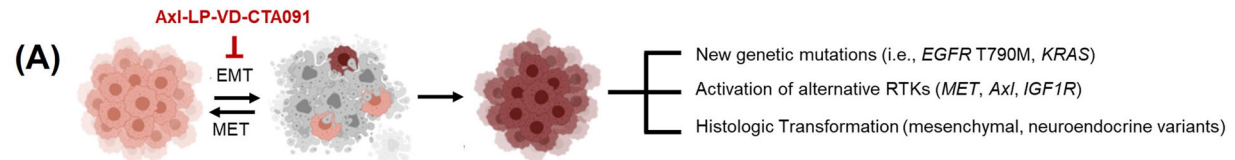
We evaluated the targeting and uptake of Axl-LP-VD-CTA091 in H1975OR cells that developed EMT-associated osimertinib tolerance (Supplementary Figure S2A). Axl aptamers were labeled with FITC. LP were labeled by encapsulation of Cy5-oligodeoxynucleotide (Cy5-ODN). H1975OR cells were incubated with vehicle, free Cy5-ODN, untargeted LP-Cy5-ODN or FITC-Axl-LP-Cy5-ODN. Intact FITC-Axl-LP-Cy5-ODN were taken up by H1975OR cells, as evidenced by co-localization of green and red fluorescence in the cytoplasm (Figure 1C). Flow cytometric quantitation demonstrated strong cellular uptake of FITC-Axl-LP-Cy5-ODN with 816.5-fold higher uptake vs. vehicle control and 40.9-fold higher uptake vs. free Cy5-ODN (Figure 1D). However, Axl aptamers did not increase uptake beyond what was achieved with non-targeted LP.

Next, we tested the prediction that Axl-LP-VD-CTA091 promoted VD signaling, decreased EMT features and improved osimertinib sensitivity in H1975OR cells. Axl-LP-VD-CTA091 induced vitamin D target gene cytochrome P450 family 24 subfamily A member 1 (*CYP24A1*), increased expression of epithelial marker cadherin 1 (*CDH1*), and decreased expression of mesenchymal marker matrix metalloproteinase-2 (*MMP2*) (Figure 1E). Axl-LP-VD-CTA091 was superior to comparator treatments, including free VD + CTA091 (demonstrating the importance of drug encapsulation to activity), Axl-LP-VD (indicating the importance of using CTA091 to stabilize VD) and

List of abbreviations: Axl-LP-VD-CTA091, Axl targeted liposomes that are loaded with VD + CTA091; Axl-LP-VD, Axl targeted liposomes that are loaded only with VD; Axl-LP, Axl targeted empty liposomes that are not loaded with VD + CTA091; *CDH1*, cadherin 1; *CYP24A1*, cytochrome P450 family 24 subfamily A member 1; Cy5-ODN, Cy5 labeled oligodeoxynucleotide; DTC, drug tolerant cell; *EGFR*, epidermal growth factor receptor; EMT, epithelial mesenchymal transition; IVIS, in vivo imaging system; LP, liposome; *MMP2*, matrix metalloproteinase-2; MRI, magnetic resonance imaging; NSCLC, non-small cell lung cancer; SRB, sulforhodamine B; TKI, tyrosine kinase inhibitor; US, ultrasound; VD, 1,25-dihydroxyvitamin D3.

This is an open access article under the terms of the [Creative Commons Attribution-NonCommercial-NoDerivs](https://creativecommons.org/licenses/by-nc-nd/4.0/) License, which permits use and distribution in any medium, provided the original work is properly cited, the use is non-commercial and no modifications or adaptations are made.

© 2022 The Authors. *Cancer Communications* published by John Wiley & Sons Australia, Ltd. on behalf of Sun Yat-sen University Cancer Center.



Axl-LP containing no VD and CTA091 (showing that Axl-aptamers and empty liposomes lack therapeutic activity). Gene expression changes induced by LP-VD-CTA091 and Axl-LP-VD-CTA091 were comparable and consistent with their similar in vitro uptake. Axl-LP-VD-CTA091 induced an 8-fold increase in *CDHI* transcripts and a corresponding 3.2-fold increase in E-cadherin protein (Figure 1E). Osimertinib dose-response studies were used to test EGFR TKI sensitivity. Axl-LP-VD-CTA091 re-sensitized H1975OR cells to treatment, as evidenced by a 3.5-fold reduction in the osimertinib EC50 value compared with Axl-LP ($P = 0.004$). The osimertinib EC50 was comparable for vehicle control (HEPES) and Axl-LP ($P = 0.625$), indicating that empty liposomes did not affect EGFR TKI sensitivity (Figure 1F). Notably, Axl-LP-VD-CTA091 were unable to increase the EGFR TKI sensitivity of PC9ER cells that did not undergo EMT and had genetically fixed erlotinib resistance (Supplementary Figure S2B-C). These data further linked Axl-LP-VD-CTA091 activity to EMT control.

To investigate the in vivo activity of Axl-LP-VD-CTA091, we developed a novel orthotopic model of lung cancer

based on ultrasound (US) guided trans-pleural injection of tumor cells into the lungs of mice (Supplementary Figure S3A-C). Nude mice were orthotopically implanted with parental H1975 cells (Supplementary Figure S3D-F) or H1975OR cells (Supplementary Figure S3G-I). Osimertinib treatment (5 mg/kg oral gavage, once daily, Mon-Fri) was initiated after tumor establishment (day 27 post-implantation) in H1975-bearing mice but within 1 week of implantation of H1975OR cells to maintain TKI tolerance. Osimertinib suppressed EGFR activation and reduced the volume of H1975 tumors (Supplementary Figure S3E-F). However, H1975OR tumors continued to grow over time despite receiving the same dose of osimertinib (Supplementary Figure S3G-H). H1975OR tumors expressed lower E-cadherin levels than parental H1975 tumors, indicating that they maintained their EMT phenotype in vivo (Supplementary Figure S3I). We concluded that osimertinib (5 mg/kg) allowed for continued growth of drug tolerant H1975OR cells with EMT phenotype in vivo.

We did not observe significant differences in cellular uptake and efficacy between Axl-LP-VD-CTA091 and

FIGURE 1 In vitro and in vivo characterization of the biological activity of Axl-LP-VD-CTA091. (A) In response to EGFR TKI treatment, most *EGFR* mt NSCLC cells die (gray). However, a subset of cells (DTCs, red) undergoes EMT and survives treatment. Over time, DTCs expand, evolve, and give rise to diverse mechanisms of EGFR TKI resistance. Axl-LP-VD-CTA091 oppose EMT and thereby prevent EGFR TKI failure. (B) Schematic representation of Axl-LP-VD-CTA091. VD (200 nmol/L) and CTA091 (100 nmol/L) were encapsulated in LP. Concentrations of each agent were determined based on prior optimization experiments. Axl aptamers decorated the surface of LP. Structural depiction is based on morphology observed in Cryo-TEM studies (Supplementary Figure S1C). (C) Untargeted LP-Cy5-ODN or targeted FITC-Axl-LP-Cy5-ODN were incubated with H1975OR cells and visualized by confocal microscopy to determine cellular uptake. Nuclei were stained with DAPI. Merged images showed the overlap in the localization of Cy5 and FITC within cells. (D) Binding of the indicated agents to H1975OR cells was determined by flow cytometry. Data were mean fluorescence intensity \pm SD for ≥ 5 technical replicates from 2 biological replicates. (E) H1975OR cells were exposed to the indicated treatments. VD and CTA091 concentrations were equal across all groups. Effects of treatment on expression of vitamin D target gene *CYP24A1* and EMT-related genes *CDHI* (epithelial marker) and *MMP2* (mesenchymal marker) were determined by qRT-PCR. Data were normalized to vehicle controls (arbitrarily set to an expression value of 1.0). Data were mean \pm SD for 3 biological replicates. Statistical significance was evaluated using one-way ANOVA with multiple comparisons using GraphPad Prism 9.3.1 software. ns, not significant; *, $P < 0.05$; **, $P < 0.01$; ****, $P < 0.0001$. Statistics were provided for each treatment vs Axl-LP-VD-CTA091. Immunoblotting was used to determine the effects of the indicated treatments on E-cadherin expression. Densitometric quantitation was indicated below blots. (F) The ability of Axl-LP-VD-CTA091 to alter sensitivity to osimertinib was tested using the SRB assay. Osimertinib dose response was measured at 9 d post-treatment. Each curve represented the average of 3 biological replicates. P value was for comparison of EC50 values for all 3 groups by ANOVA. (G) Representative IVIS and MR images of a mouse harboring an H1975 orthotopic xenograft. Images were obtained prior to treatment (MRI) or 1 h or 24 h post-treatment with untargeted LP-Cy5-ODN or tumor-targeted Axl-LP-Cy5-ODN. Yellow circles in MR images highlighted lung tumors. (H) In vivo biodistribution of Cy5 detected by IVIS Optical Imaging. The percent Cy5 signal present was calculated per organ at each time point from IVIS images. Data were mean \pm SD for $n = 3$ mice per group. The indicated organs were harvested at the time of euthanasia from $n = 3$ mice per group and immediately imaged by IVIS. The proportion of Cy5 signal detected per organ basis was indicated in pie charts. LU, lung; KI, kidney; LI, liver; SP, spleen. (I) Tumor outgrowth curves were presented for mice harboring H1975OR orthotopic xenografts. Osimertinib was initiated at d 7 in all mice and continued throughout the study. Axl-LP, free VD+CTA091 and Axl-LP-VD-CTA091 were administered every other day, beginning on d 57 post-implantation. MRI-detected tumor volume was presented as mean \pm SD for $n = 4$ mice per group. Statistical significance was evaluated using 2-way ANOVA with GraphPad Prism 9.3.1 software. *, $P < 0.050$; **, $P < 0.010$. (J) Body weight determination in mice stratified to treatment with Axl-LP, free VD+CTA091, or Axl-LP-VD-CTA091. For each group, body weight at d 57 (prior to treatment initiation) was set to baseline (100%). (K) At study termination, blood was collected from all animals and used to measure serum calcium levels via colorimetric assay. Data were mean \pm SD for $n = 4$ mice per group. Statistical significance was evaluated using one-way ANOVA with multiple comparisons using GraphPad Prism 9.3.1 software. *, $P < 0.050$; **, $P < 0.010$; ns, not significant. Abbreviations: d, day; EGFR, epidermal growth factor receptor; TKI, tyrosine kinase inhibitor; NSCLC, non-small cell lung cancer; EMT, epithelial-mesenchymal transition; DTC, drug-tolerant cell; VD, 1,25-dihydroxyvitamin D3; LP, liposomes; SRB, sulforhodamine B; MRI, magnetic resonance imaging; IVIS, in vivo imaging system; SD, standard deviation.

untargeted LP-VD-CTA091 *in vitro*. One possible reason could be that *in vitro* culture conditions do not mimic *in vivo* conditions and lack blood flow, competing cells and off-target effects. To test for advantages of Axl-LP-VD-CTA091 over LP-VD-CTA091 *in vivo*, biodistribution studies were performed. Untargeted LP-Cy5-ODN or Axl-LP-Cy5-ODN were administered to mice harboring orthotopic H1975 xenografts at a Cy5-ODN dose of 5 mg/kg (Figure 1G-H). H1975 cells were used for biodistribution studies because they expressed Axl (Supplementary Figure S2A) and grew relatively rapidly. *In vivo* imaging system (IVIS) was used to quantify LP distribution over time. An intense fluorescent signal was detected within 1 h of administration in mice that received Axl-LP-Cy5-ODN (Figure 1G). The Cy5 signals were detected preferentially in the tumor-bearing lung. No specific localization was detected in mice that received LP-Cy5-ODN, despite the mice having comparable tumor burden. Quantitative *in vivo* analyses confirmed signal enrichment in the lungs of Axl-LP-Cy5-ODN treated mice at the 1 h timepoint, which was significantly higher than mice treated with LP-Cy5-ODN (71% vs. 58%, Figure 1H). After 24 h treatment, the majority of fluorescent signal (40%) was present in the lungs of Axl-LP-Cy5-ODN injected mice, while only 13% of fluorescent signal remained in the lungs of LP-Cy5-ODN treated mice (Figure 1G-H). In addition, the kidney and liver showed greater signal intensities than the lungs of LP-Cy5-ODN-treated mice. The relative enrichment of Axl-LP-Cy5-ODN in lung tissues was evident when isolated organs were subjected to IVIS imaging (Figure 1H, pie charts). The lung/kidney Cy5 signal intensity ratio was 2.58 and 0.5 in mice that received Axl-LP-Cy5-ODN versus LP-Cy5-ODN, respectively. Thus, Axl-targeting resulted in preferential localization and retention of LP within the lungs of tumor-bearing mice.

Based on these results, we conducted *in vivo* safety and efficacy tests of Axl-LP-VD-CTA091. H1975OR cells were orthotopically implanted. One week later, treatment with osimertinib was initiated. Once tumors were established (day 57 post-implantation), the mice were intravenously injected with empty Axl-LP, free VD + CTA091, or Axl-LP-VD-CTA091 at VD and CTA091 doses of 25 $\mu\text{g}/\text{kg}$ and 14.5 $\mu\text{g}/\text{kg}$ respectively, every 2 days, for a total of 4 injections. Magnetic Resonance Imaging (MRI)-based tumor volume measurements showed that Axl-LP-VD-CTA091 significantly suppressed the growth of H1975OR lung tumors in mice compared to treatment with Axl-LP or free VD + CTA091 (Figure 1I). However, the mice began to lose weight following treatment with Axl-LP-VD-CTA091 and free VD + CTA091, prompting us to terminate the study (Figure 1J). Weight loss was associated with an elevation in serum calcium, indicative of hypercalcemia (Figure 1K). Pathological assessments revealed no overt tissue toxicity

(data not shown). Axl-LP-VD-CTA091 but not free VD + CTA091 reduced tumor burden; therefore, we anticipated that the therapeutic index of Axl-LP-VD-CTA091 might be improved using reduced drug doses and/or an alternative once-weekly dosing schedule.

Based on the ability of Axl-LP-VD-CTA091 to promote epithelial phenotype, distribute to tumor-bearing lungs *in vivo*, and increase EGFR TKI activity *in vitro* and *in vivo*, we contend that its continued additional evaluation as a novel strategy to inhibit DTC and promote EGFR TKI sensitivity is warranted.

AUTHORS CONTRIBUTIONS

Tatiana Shaurova: study design, model development, data generation, manuscript writing, and editing.

Lingyue Yan: study design, nanoparticle synthesis, data generation, manuscript writing, and editing.

Yafei Su: nanoparticle synthesis and data generation.

Laurie James Rich: co-development of orthotopic tumor models.

Vui King Vincent-Chong: immunohistochemistry.

Hannah Calkins: data generation, manuscript writing, and editing.

Saraswati Pokharel: pathologic assessment of tissues.

Martin Petkovich: synthesis and provision of CTA091, manuscript editing.

Mukund Seshadri: co-development of orthotopic tumor models, manuscript writing, and editing.

Yun Wu: study design, data generation, manuscript writing, and editing.

Pamela Anne Hershberger: study design, data generation, manuscript writing, and editing.

ACKNOWLEDGMENTS

We thank Dr. Min Gao and the TEM facility at the Advanced Materials and Liquid Crystal Institute at Kent State University for Cryo-TEM images.

COMPETING INTERESTS

Laurie James Rich is currently an employee of Fujifilm-VisualSonics Corporation. The remaining authors declare no competing financial interest.

FUNDING

The authors gratefully acknowledge the following sources of funding support for our work: the Roswell Park Alliance Foundation (Taste of Life Award), the American Lung Association Lung Cancer Discovery Award LCD615335, S10OD010393-01, and the Roswell Park Cancer Center Support Grant P30 CA016056 that supports the Laboratory Animal Shared Resource and Translational Imaging Shared Resource utilized in this work. The Zeiss LSM

710 confocal microscope at University at Buffalo North Campus Imaging Facility was funded by National Science Foundation Major Research Instrumentation Grant # DBI 0923133.

AVAILABILITY OF DATA AND MATERIALS

Primary data will be made available upon request to the corresponding authors.

ETHICS APPROVAL AND CONSENT TO PARTICIPATE

In vivo studies were carried out under an IACUC-approved protocol (1213M) within the laboratory animal resource at Roswell Park Comprehensive Cancer Center.

CONSENT FOR PUBLICATION

Not applicable.

Tatiana Shaurova^{1,†}
 Lingyue Yan^{2,†}
 Yafei Su²
 Laurie James Rich^{3,4}
 Vui King Vincent-Chong⁵
 Hannah Calkins¹
 Saraswati Pokharel⁶
 Martin Petkovich⁷
 Mukund Seshadri⁵ 
 Yun Wu² 
 Pamela Anne Hershberger¹ 

¹*Department of Pharmacology and Therapeutics, Roswell Park Comprehensive Cancer Center, Buffalo, New York, USA*

²*Department of Biomedical Engineering, University at Buffalo, the State University of New York, Buffalo, New York, USA Email: lingyue556@gmail.com*

³*Cell Stress and Biophysical Oncology Graduate Program, Roswell Park Comprehensive Cancer Center, Buffalo, New York, USA*

⁴*Fujifilm-VisualSonics Corporation, Toronto, Ontario, Canada*

⁵*Department of Oral Oncology, Roswell Park Comprehensive Cancer Center, Buffalo, New York, USA*

⁶*Department of Pathology, Roswell Park Comprehensive Cancer Center, Buffalo, New York, USA*

⁷*Cancer Research Institute, School of Medicine, Queens University, Kingston, Ontario, Canada*

Correspondence

Yun Wu
 Email: ywu32@buffalo.edu

Pamela Anne Hershberger


Email: pamela.hershberger@roswellpark.org

[†]These authors contributed equally to this work.

ORCID

Mukund Seshadri  <https://orcid.org/0000-0001-8729-9532>

Yun Wu  <https://orcid.org/0000-0002-6926-777X>

Pamela Anne Hershberger  <https://orcid.org/0000-0003-0030-6520>

REFERENCES

- Zhou C, Wu YL, Chen G, Feng J, Liu XQ, Wang C, et al. Erlotinib versus chemotherapy as first-line treatment for patients with advanced EGFR mutation-positive non-small-cell lung cancer (OPTIMAL, CTONG-0802): a multicentre, open-label, randomised, phase 3 study. *Lancet Oncol.* 2011;12(8):735-42.
- Soria JC, Ohe Y, Vansteenkiste J, Reungwetwattana T, Chewaskulyong B, Lee KH, et al. Osimertinib in untreated EGFR-mutated advanced non-small-cell lung cancer. *The N Engl J Med.* 2018;378(2):113-25.
- Passaro A, Janne PA, Mok T, Peters S. Overcoming therapy resistance in EGFR-mutant lung cancer. *Nat Cancer.* 2021;2(4):377-91.
- Sharma SV, Lee DY, Li B, Quinlan MP, Takahashi F, Maheswaran S, et al. A chromatin-mediated reversible drug-tolerant state in cancer cell subpopulations. *Cell.* 2010;141(1):69-80.
- Ramirez M, Rajaram S, Steininger RJ, Osipchuk D, Roth MA, Morinishi LS, et al. Diverse drug-resistance mechanisms can emerge from drug-tolerant cancer persister cells. *Nat Commun.* 2016;7:10690.
- Hata AN, Niederst MJ, Archibald HL, Gomez-Caraballo M, Siddiqui FM, Mulvey HE, et al. Tumor cells can follow distinct evolutionary paths to become resistant to epidermal growth factor receptor inhibition. *Nat Med.* 2016;22(3):262-9.
- Shaurova T, Dy GK, Battaglia S, Hutson A, Zhang L, Zhang Y, et al. Vitamin D3 metabolites demonstrate prognostic value in EGFR-mutant lung adenocarcinoma and can be deployed to oppose acquired therapeutic resistance. *Cancers (Basel).* 2020;12(3):675.
- Zhang Q, Kanterewicz B, Buch S, Petkovich M, Parise R, Beumer J, et al. CYP24 inhibition preserves 1alpha,25-dihydroxyvitamin D(3) anti-proliferative signaling in lung cancer cells. *Mol Cell Endocrinol.* 2012;355(1):153-61.
- Cerchia L, Esposito CL, Camorani S, Rienzo A, Stasio L, Insabato L, et al. Targeting Axl with an high-affinity inhibitory aptamer. *Mol Ther.* 2012;20(12):2291-303.
- Taniguchi H, Yamada T, Wang R, Tanimura K, Adachi Y, Nishiyama A, et al. AXL confers intrinsic resistance to osimertinib and advances the emergence of tolerant cells. *Nat Commun.* 2019;10(1):259.

SUPPORTING INFORMATION

Additional supporting information can be found online in the Supporting Information section at the end of this article.